Journal of Electroceramics 2:4, 257–272, 1998

Piezoelectric Sensors and Sensor Materials

JAMES F. TRESSLER, SEDAT ALKOY & ROBERT E. NEWNHAM
Materials Research Laboratory, The Pennsylvania State University, University Park, PA 16802

Submitted November 3, 1997; Revised March 25, 1998; Accepted March 31, 1998

Abstract. This paper reviews the current trends and historical development of piezoelectric sensors and sensor materials technology. It begins with a discussion of the bases of piezo- and ferroelectric activity, followed by an overview of the most commonly used piezoelectric ceramic: lead zirconate titanate (PZT). A discussion of the properties and applications of piezoelectric crystals and additional piezoelectric ceramics is followed by a description of several sensor configurations prepared from bulk ceramics. An extensive review and comparison of piezoelectric ceramic—polymer composite sensors based on the connectivity of the constituent phases is also presented. We conclude our discussion of sensor configurations with recent examples of piezoelectric ceramic—metal composite sensors, and expected future developments in the area of piezoelectric sensors.

Keywords: piezoelectricity, ferroelectricity, sensors, PZT, piezoelectric ceramics, piezoelectric crystals, piezaelectric compsites, connectivity

1. Introduction

Piezoelectricity is a phenomenon exhibited by non-centrosymmetric crystals whereby an electric polarization (i.e. charge) is induced in the material upon the application of a stress. Conversely, it is the development of an induced strain which is directly proportional to an applied electric field. The latter phenomenon is known as the converse effect and is utilized in actuation. The former is called the direct effect and is used in sensing dynamic pressure changes, changes in acceleration (from shock or vibration), and changes in force [1]. Whether a material that belongs to one of the piezoelectric point groups actually exhibits measurable piezoelectricity has to be measured experimentally [2].

Through proper design and selection of materials, the frequency range that piezoelectric materials can detect changes in force or motion can range from below 1 Hz to above several MHz. Displacements in the μm range can be precisely measured as can force changes from mN to kN. The rugged solid-state construction of industrial piezoelectric ceramic sensors enables them to operate under most harsh environmental conditions, including dirt, oil, and most chemical atmospheres. They perform well over a wide temperature range and resist damage from severe shock and/or vibration [3].

Piezoelectricity exists in some naturally occurring crystals such as quartz and rochelle salt, and it can be induced in polymers such as nylon and copolymers of vinylidene fluoride (VDF) with trifluoroethylene (TrFE), or with tetrafluoroethylene (TeFE) [4]. However, the bulk of the piezoelectric materials used for commercial sensing applications come from synthetic polycrystalline ferroelectric ceramics, such as PZT. Compared to single crystals ceramics offer the advantage of high strength and ease of fabrication in general, especially into complex shapes and large area pieces. This paper will review the significant piezoelectric ceramic sensor materials, composite sensor configurations, and some typical applications.

2. Ferroelectricity

Ferroelectrics are a class of piezoelectric materials that exhibit a spontaneous polarization that is reorientable under a realizable electric field ($\approx 10^6$ V/m). Ferroelectric oxides with the perovs-

kite, tungsten bronze, pyrochlore, and bismuth titanate layer structures all have high dielectric constants and high electromechanical coupling coefficients. In addition, all contain corner-linked octahedral networks of Ti^{4+}, Nb^{5+}, or other d^0 ions. These transition-metal elements are the highly polarizable ''active'' ions promoting ferroelectricity and the high permittivity and piezoelectric constants required for sensing. With reference to the periodic table, there are two major groups of active ions, both of which are near electronic ''crossover'' points where different types of atomic orbitals are comparable in energy and where hybrid bond formation is prevalent. The first group, typified by Ti^{4+}, Nb^{5+}, and W^{6+}, consists of d^0 ions octahedrally coordinated to oxygen. For Ti^{4+}, the electronic crossover involves the 3*d*, 4*s*, and 4*p* orbitals, which combine with the sigma and pi orbitals of its six O^{2-} neighbors to form the $(TiO_6)^{8-}$ complex. The bond energy of the complex can be lowered by distorting the octahedron to a lower symmetry. This leads to molecular dipole moments, ferroelectricity, large dielectric constants, and piezoelectricity. A second group of active elements contributing to polar distortions in ceramic dielectrics are the lone-pair ions having two electrons outside a closed shell in an asymmetric hybrid orbital. Among oxides, the most important of these lone-pair ions are Pb^{2+} and Bi^{3+}, which are involved in a number of ferroelectrics ($PbTiO_3$, $Bi_4Ti_3O_{12}$, $PbNb_2O_6$) with high Curie temperatures. In many of these compounds, Pb^{2+} and Bi^{3+} are in pyramidal coordination with oxygen and therefore contribute to the spontaneous polarization [5].

3. Piezoelectric PZT

Most piezoelectric ceramic sensor formulations are based on PZT (a registered trademark of Clevite Corporation), which has become a common acronym for the solid solutions of nominal composition 52–54 mole % lead zirconate ($PbZrO_3$) and 46–48 mole% lead titanate ($PbTiO_3$). PZT is one of a number of ferroelectric substances crystallizing with the perovskite structure. Lead atoms are positioned at the corners of the unit cell and oxygens at the face centers. Both lead and oxygen ions have radii of about 1.4 Å. Together they make up a face-centered cubic array, having a lattice parameter of about 4 Å. Octahedrally coordinated titanium or zirconium ions are located at the center of the unit cell.

Upon cooling from high temperature, the crystal structure of PZT undergoes a displacive phase transformation with atomic displacements of about 0.1 Å. For titanium-rich compositions, the point symmetry changes from cubic m3m to tetragonal 4 mm at the Curie temperature. The tetragonal state with its spontaneous polarization along [001] persists to 0°K. These structural changes are shown in Fig. 1.

To make use of these piezoelectric ceramics with their large polarizations, compositions near a second phase transition are chosen. At the Curie point, PZT converts from a paraelectric state with the cubic perovskite structure to a ferroelectric phase located near a morphotropic phase boundary between the tetragonal and rhombohedral states. Very large piezoelectric coupling between electric and mechanical variables is obtained near this phase boundary.

Polycrystalline ferroelectric ceramics (Curie point group $\infty\infty$m) such as PZT initially contain randomly oriented polarized regions within each grain called domains. These domains form upon cooling through the Curie temperature in order to minimize the total elastic energy in the ceramic [2]. Because of this polarization randomness, polycrystalline ferroelectrics do not exhibit the piezoelectric effect. Piezoelectricity can be induced, however, by applying a static electric field larger than the saturation field but

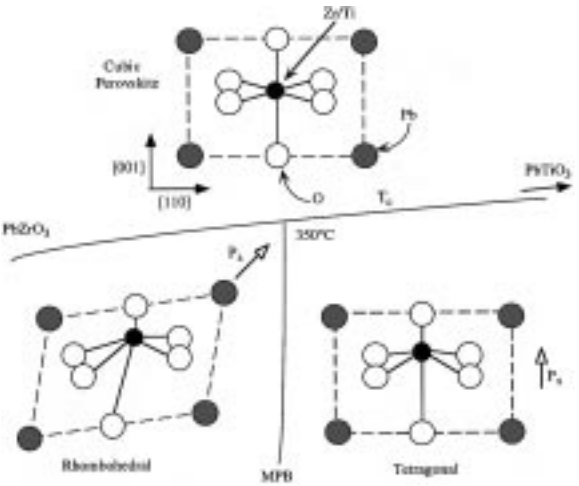

Fig. 1. A portion of the the $PbZrO_3$—$PbTiO_3$ phase diagram showing the structural changes at the Curie temperature and the morphotropic phase boundary (MPB). Compositions near the morphotropic phase boundary have 14 possible poling directions.

smaller than the breakdown field at elevated temperatures below the ferroelectric Curie point where the domains are easily aligned. This process is known as poling. Poling orients the domains by reversal, or by a change through angles that depend on the crystal structure so that the spontaneous polarization has a component in the direction of the poling field [6] and imparts conical symmetry (∞m). When the electric field is removed, some of the more highly strained domains revert to their initial position (depolarization), but a large majority remain aligned (remnant polarization), resulting in the material being permanently poled.

For a poled ceramic having symmetry ∞m, d_{31}, d_{33}, and d_{15} are the appropriate tensor coefficients. Both intrinsic and extrinsic contributions to these piezoelectric coefficients exist. The intrinsic effects coming from the distortions of the crystal structure under mechanical stress appear in Fig. 2. Under mechanical stress parallel to the dipole moment, there is an enhancement of the spontaneous polarization P_s along x_3. This is the d_{33} effect. When stress is applied perpendicular to the dipole moment, electric charges develop transversely, and this is called the d_{31} effect. When the dipole is tilted by shear stress, charges appear on the side faces, leading to the d_{15} coefficient. There are extrinsic contributions to the piezoelectric coefficient as well. These can be extremely large, often involving the domain wall motions.

Titanium-rich compositions in the PZT system

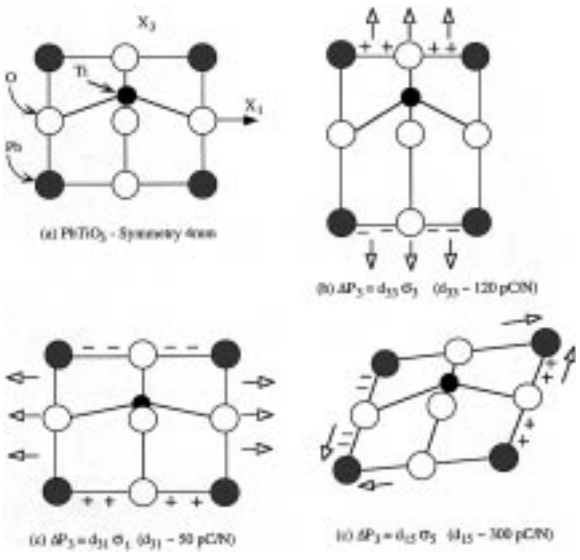

Fig. 2. Intrinsic piezoelectric effect in polar lead titanate.

favor a tetragonal modification with sizable elongation along [001] (for a total of six equivalent directions) and a large spontaneous polarization in the same direction. A rhombohedral ferroelectric state is favored for zirconium-rich compositions. In this case, the polarization and distortion are along [111], giving rise to eight possible equivalent domain states. The compositions that pole best lie near the morphotropic boundary between the rhombohedral and tetragonal ferroelectric phases. For these compositions, there are 14 possible equivalent poling directions over a very wide temperature range (-50°C to $+200$°C). This explains in part why the ceramic piezoelectric coefficients are largest near the morphotropic boundary. Phase changes between the rhombohedral and tetragonal phases also occur during the poling process [5].

The addition of dopants to PZT can have a profound impact on its properties. Donor dopants cause cation (metal) vacancies in the crystal structure which enhance domain reorientation and hence the extrinsic contribution to the piezoelectric coefficients. As a result, these electrically ''soft'' PZTs (such as those designated as 5A and 5H) have large piezoelectric coefficients, large permittivity, high electrical losses, large electromechanical coupling factors, very high electrical resistance, low mechanical quality factors, and a low coercive field [7]. Acceptor dopants, on the other hand, cause oxygen vacancies. These oxygen vacancies pin the domain walls, with the defect dipoles aligning with the spontaneous polarization within a domain [2]. This leads to an electrically ''hard'' PZT (e.g. those with designations 4 and 8). A hard PZT is characterized by low piezoelectric coefficients, low permittivity, low losses, low electrical resistivity, high Q_m, and a high coercive field [8]. Isovalent substitutions tend to reduce the Curie temperature and hence increase the room temperature permittivity [9]. Multivalent ions, which substitute for either Ti^{4+} or Zr^{4+}, serve to reduce aging effects [10]. A listing of the more commonly used dopants is provided in Table 1.

4. Sensor Characterization

The sensitivity of a piezoelectric is taken to be equal to the open circuit voltage that it generates due to an applied stress, or $g{\cdot}t$, where ''g'' is the relevant piezoelectric voltage tensor and ''t'' is the thickness of

Table 1. Listing of common ion substitutions in PZT [8,66]

Pb-site donors :	La^{3+}, Bi^{3+}, Nd^{3+}, Sb^{3+}, Th^{4+}
(Ti-Zr)-site donors:	Nb^{5+}, Ta^{5+}, Sb^{5+}, W^{6+}
Pb-site acceptors:	K^{+}, Na^{+}, Rb^{+}
(Ti-Zr)-site acceptors:	Fe^{3+}, Al^{3+}, Sc^{3+}, In^{3+}, Cr^{3+}, Co^{3+}, Ga^{3+}, Mn^{3+}, Mn^{2+}, Mg^{2+}, Cu^{2+}
isovalent substitutions:	Sr^{2+}, Ca^{2+}, Ba^{2+} (for Pb^{2+}), Sn^{4+} (for Ti^{4+} or Zr^{4+})
multivalent ions:	Cr, U

the piezoelectric element. The sensitivity needs to be sufficiently high so that the generated signal can be detected above the background noise. In practice, the generated signal is small and has to be enhanced by an appropriate charge or voltage amplifier. The sensitivity is maximized when the ''g'' coefficient is maximized. The ''g'' coefficient is related to the ''d'' coefficient through the dielectric constant, K, as follows: $g = d/K\varepsilon_o$, where ε_o is the permittivity of free space. Typically, a large dielectric constant, or capacitance, is also desirable for sensors in order to overcome the losses associated with the cables. Unfortunately, an increase in dielectric constant results in a lower voltage coefficient, as seen in the aforementioned equation. Another important parameter of a piezoelectric material is the electromechanical coupling coefficient, k which can be defined
as; $k^2 =$ (stored mechanical energy/input electrical energy)
or $k^2 =$ (stored electrical energy/input mechanical energy)

When operating in the hydrostatic mode, i.e. when the incident stress is equal on all sides, the tensor coefficients are represented as $d_h = d_{33} + 2d_{31}$ and $g_h = g_{33} + 2g_{31}$. A figure-of-merit, the $d_h \cdot g_h$ product, is often reported as a measure of the quality of the sensing capability of the piezoelectric element or to compare different hydrophone materials [11]. Quantitatively, it is used to ascertain the type of amplifier required in the electronic circuitry to overcome the self-noise of the system, and in the case of composites should be normalized by the volume of the device in order to make accurate comparisons [12].

5. Piezoelectric Sensor Materials

5.1. *Crystals*

Although some piezoelectric crystals, such as quartz and rochelle salt, occur in nature, they are more commonly grown synthetically. To be of practical use, however, they have to be oriented and cut along specific crystallographic directions so as to obtain the best piezoelectric response. A listing of the more significant piezoelectric crystals, along with their best piezoelectric coefficient, is given in Table 2.

Quartz is still used quite extensively in accelerometers [1]. Lithium sulfate (because of its large g_h coefficient) and tourmaline are two piezoelectric crystals still used in commercial hydrophones, the latter earmarked for shock and blast measurements [13]. Rochelle salt still sees some limited use on one type of sonic blast sensor [13]. Lithium niobate ($LiNbO_3$) and lithium tantalate ($LiTaO_3$) are both used as high temperature acoustic sensors because they both maintain high sensitivity up to 400°C [14]. Other high-temperature piezoelectric crystals with good thermal stability include the perovskite layer structure (PLS) ferroelectrics such as $Sr_2Nb_2O_7$ and $La_2Ti_2O_7$ which have Curie temperatures of 1342°C and 1500°C, respectively [14]. Polar glass ceramics, which are grown by conventional crystal growing techniques, are of interest for hydrophone applications [14]. Because of their very stable piezoelectric properties, natural crystals are best suited for sensor applications in which a variable has to be monitored over long periods of time [1].

5.2. *Ceramics*

The first polycrystalline ferroelectric ceramic was barium titanate ($BaTiO_3$), which has the perovskite structure, and was discovered independently by researchers in the United States, Japan, and the Soviet Union in 1943. Its superiority over single crystals was recognized immediately and it remained the primary electroceramic material until the discovery of lead zirconate titanate (PZT) in 1954 by Jaffe et al. [9,15].

The solid solution of lead zirconate and lead titanate (PZT), which also has the perovskite crystal

Table 2. Room temperature properties of common piezoelectric crystals

Crystal name	Chemical formula	Point group	Max. piezoelec. charge coef. (pC/N)		Dielectric constant K_{11}^T	Dielectric constant K_{33}^T	Ref.
Amonium Dihydrogen Phosphate (ADP)	$NH_4H_2PO_4$	$\bar{4}2m$	50.0	(d_{36})	55.0	15.0	[67]
Barium Sodium Niobate (BNN)	$Ba_2NaNb_5O_{15}$	mm2	52.0	(d_{24})	246.0	51.0	[66,67]
Barium Titanate	$BaTiO_3$	4mm	392.0	(d_{15})	2920.0	168.0	[67]
Ethylene Diamine Tartrate (EDT)	$C_6H_{14}N_2O_6$	2	− 12.3	(d_{23})	5.0	6.0	[67]
Lead Barium Niobate (PBN)	$Pb_{0.37}Ba_{0.63}Nb_2O_6$	4mm	108.0	(d_{15})	600.0	135.0	[66]
Lead Potassium Niobate (PKN)	$Pb_2KNb_5O_{15}$	mm2	470.0	(d_{15})	1550.0	129.0	[67]
Lead Niobate	$PbNb_2O_6$	mm2	45.0	(d_{33})	—	180.0	[67]
Lithium Niobate	$LiNbO_3$	3m	68.0	(d_{15})	84.0	30.0	[15,66]
Lithium Sulfate	$LiSO_4{\cdot}H_2O$	2	16.2	(d_{22})	5.6	6.5	[67]
Lithium Tantalate	$LiTaO_3$	3m	26.0	(d_{15})	51.0	45.0	[15,66]
Quartz	SiO_2	32	2.3	(d_{11})	4.6	4.7	[67]
Potassium Dihydrogen Phosphate (KDP)	KH_2PO_4	$\bar{4}2m$	23.2	(d_{36})	44.0	21.0	[66,67]
Rochelle Salt	$NaKC_4H_4O_6{\cdot}4H_2O$	222	2300.0	(d_{14})	1100.0	9.2	[66,67]
Sodium Chlorate	$NaClO_3$	23	1.7	(d_{14})	5.8		[67]
Triglycine Sulfide (TGS)	$(NH_2CH_2COOH)_3{\cdot}H_2SO_4$	2	25.3	(d_{23})	8.6	5.7	[66,67]
Tourmaline	$CaAl_3Mn_6(BO_3)_3(SiO_3)_6(OH)_4$	3m	3.6	(d_{15})	8.2	7.5	[67]
Zinc Sulfide	ZnS	6mm	3.2	(d_{33})	8.6	8.0	[67]

structure, was described previously. A complete description of its piezoelectric properties is shown in Table 3. While individual manufacturers of PZT use proprietary formulas for each composition, in general, PZT-5 is Nb-doped, PZT-6 is Cr-doped, PZT-7 is La-doped, and PZT-4 is Fe-doped [15]. Often, PZT types are reported by their US Navy designations as Type I, II, or III. Type I is a hard PZT with a T_c greater than or equal to 310°C. Type II is a soft PZT with a Curie temperature of greater than or equal to 330°C. Type III is a very hard PZT with a T_c of greater than or equal to 290°C. Type IV is barium titanate with nominal additives of 5% calcium titanate and 0.5% cobalt carbonate as necessary to obtain a Curie temperature of greater than or equal to 100°C [13]. A list of other important piezoceramic sensor materials and their properties is given in Table 4.

Pure lead titanate is often used as a hydrophone material when it is doped with either calcium or strontium [16]. This is because of its strong piezoelectric anisotropy. When doped with other elements, it is used as a knock sensor in automobiles. The higher operating temperature range of lead titanate allows it to be mounted closer to the combustion chamber, thus

Table 3. Properties of Lead Zirconate Titanate (PZT) ceramics

Designation	T_c (°C)	d_{33} (pC/N)	d_{31} (pC/N)	d_{15} (pC/N)	K_{33}^T	k_{33}	k_{31}	k_{15}	Ref.
PZT-2	370	152	− 60	440	450	0.63	− 0.28	0.70	[67]
PZT-4	325	285	− 122	495	1300	0.70	− 0.33	0.71	[68]
PZT-4D	320	315	− 135	n/a	1450	0.71	− 0.34	n/a	[68]
PZT-5A	365	374	− 171	585	1700	0.71	− 0.34	0.69	[68]
PZT-5B	330	405	− 185	564	2000	0.66	− 0.34	0.63	[68]
PZT-5H	195	593	− 274	741	3400	0.75	− 0.39	0.68	[68]
PZT-5J	250	500	− 220	670	2600	0.69	− 0.36	0.63	[68]
PZT-5R	350	450	− 195	n/a	1950	n/a	− 0.35	n/a	[68]
PZT-6A	335	189	− 80	n/a	1050	0.54	− 0.23	n/a	[67]
PZT-6B	350	71	− 27	130	460	0.37	− 0.15	0.38	[67]
PZT-7A	350	153	− 60	360	425	0.67	− 0.30	0.68	[68]
PZT-7D	325	225	− 100	n/a	1200	n/a	− 0.28	n/a	[68]
PZT-8	300	225	− 97	330	1000	0.64	− 0.30	0.55	[68]

Table 4. Properties of other common piezoelectric ceramics

Chemical formula	Cryst. struct.[#]	T_c (°C)	K_{33}^T (pC/N)	d_{33} (pC/N)	d_{31} (pC/N)	d_{15}	k_{33}	k_{31}	k_{15}	Ref.
$BaTiO_3$	P	115	1700	190	−78	260	0.50	0.21	0.48	[67]
$PbTiO_3$	P	470	190	56	—	68	0.45	—	—	[14]
$PbNb_2O_6$	TB	570	225	85	9	—	0.38	>0.045	—	[17,67]
$KNaNb_2O_6$	TB	420	495	127	−51	306	0.60	−0.27	−0.46	[67]
$Ba_{0.4}Pb_{0.6}Nb_2O_6$	TB	260	1500	∼220	−90	—	∼0.55	∼0.22	—	[67]
$LiNbO_3$	C	1150	25	6	—	69	0.23	—	0.60	[14]
$Na_{0.5}Bi_{0.5}Ti_2O_5$	B	320	300	∼70	∼15	—	∼0.40	∼0.10	—	[67]

[#]P: Perovskite, TB: Tungsten Bronze, C: Corundum, B: Bismuth.

giving it a faster response time as compared to PZT [14].

Three component ceramics consist of lead zirconate and lead titanate along with a third component, typically lead magnesium niobate, $Pb(Mg_{1/3}Nb_{2/3})O_3$ [17]. These piezoelectric ceramics offer several of the same advantages as do the PZT and they are quite competitive with the PZT's in terms of the piezoelectric properties.

Turner et al., reviewed a number of other piezoelectric ceramic materials that can be used for sensor applications, especially at high temperatures [14]. A synopsis of the findings is presented here. Modified bismuth titanate, with the composition $Na_{0.5}Bi_{4.5}Ti_4O_{15}$, has a layered structure and can be used for accelerometers at temperatures up to 400°C. Lead metaniobate, $PbNb_2O_6$, a member of the tungsten bronze family, is often used in nondestructive testing, medical diagnostic imaging, and for deep submergence hydrophones [13]. However, problems such as a high level of porosity and relatively low mechanical strength are often encountered in its use. Another niobate—sodium potassium niobate $(NaK)Nb_2O_6$ has seen use for high frequency transducer applications (10–200 MHz) [17]. Antimony sulfur iodide (SbSI) has a very high g_h coefficient, especially when it is modified with 4–8% oxygen, making it attractive for hydrophone applications. Unfortunately, its Curie temperature is only about 34°C, above which it loses its piezoelectric properties [13].

6. Sensor Configurations

When operated in a hydrostatic environment, bulk piezoelectric ceramics are typically poor choices as underwater acoustic sensors in the audio to low ultrasonic frequency range (i.e. < 100 kHz). As receivers, the sensitivity is low because of the crystal symmetry of the poled ceramic. The piezoelectric charge coefficient in the hydrostatic mode, d_h, is equal to the sum $d_{31} + d_{32} + d_{33}$ of the ceramic. However, $d_{31} = d_{32}$, and for the various PZT compositions, $d_{33} \approx -2d_{31}$; therefore, d_h is nearly zero [18]. As mentioned before, the piezoelectric voltage coefficient, g_h, is equal to $d_h/K\varepsilon_o$, where K is the dielectric constant and ε_o is the permittivity of free space. Since K for most ferroelectric ceramics is very large (< 1000), the g_h coefficient subsequently small. As a consequence, the voltage generated by an incoming pressure wave is very low. In order to improve the electroacoustic performance of a poled ceramic, it must be configured in such a way so that the effect of the hydrostatic pressure is minimized. This usually takes the form of air backing one side of the ceramic element, encapsulating part of the ceramic in a soft polymer to absorb a portion of the hydrostatic stress, or incorporating air spaces into the transducer itself. The primary piezoelectric sensor configurations are described below and are shown in Fig. 3.

6.1. *Bars, Disks, and Cylinders*

Bars, disks, and cylinders (free-flooded rings), shown in Fig. 3, are the simplest practical structures for electroacoustic transducers. They can be manufactured either as continuous units or as a compilation of segments, where the segmented cylinder is called a barrel-stave or a ring- stave transducer. The fundamental resonance of these structures is dictated mainly by their dimensions. In order to obtain a resonance in the audio to low ultrasonic frequency range, these transducers are required to be on the order

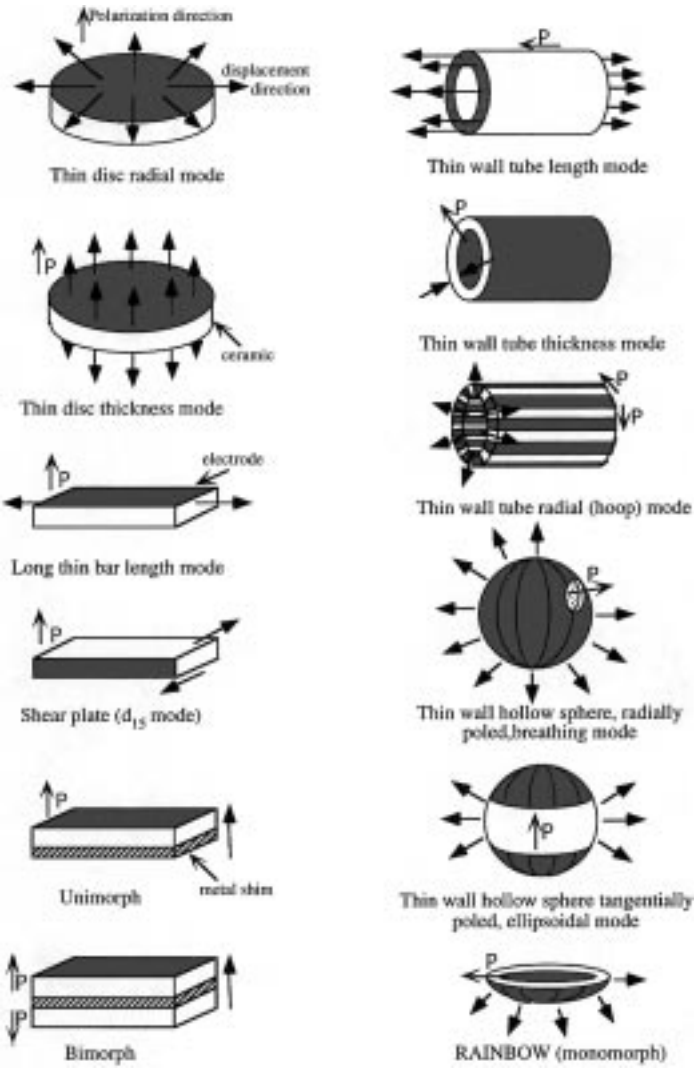

Fig. 3. Sensor configurations.

of several meters long or in diameter and consequently weigh hundreds to thousands of kilograms. Since hydrophones are operated well below their fundamental resonance, these configurations can be used as underwater receivers, provided a portion of the transducer is acoustically shielded from the effects of a hydrostatic pressure wave.

6.2. *Spheres*

Spherical designs are most often used when omnidirectional reception is required. Macro-spheres can be constructed by adhering two radially poled hemispheres back-to-back or by gluing triangular-shaped ceramic plates together into a quasi-spherical shape where the plates are poled through their thickness direction [19].

Miniature piezoelectric hollow sphere transducers, also known as BBs due to their similarity in size to the pellets used in buckshot, have a nominal diameter of 2.76 mm and a wall thickness of 80 μm [20]. They are made by the patented Torobin process. A fine slurry of PZT is prepared and injected through a coaxial nozzle to form a hollow cylinder. The bottom later closes due to surface tension and hydrostatic pressure. The closed cylinder is inflated into a bubble by the inner

air pressure until this pressure equals the surface tension of the cylinder. At this critical pressure, the bubble closes and the sphere breaks free. By changing the viscosity of the slurry and the air jet velocity, the sphere diameter and wall thickness can be tailored between 1 to 6 mm and 12–150 μm, respectively [21].

Two poling configurations have been studied: radial and top-to-bottom, and they are shown in Fig. 3. In the radial poling configuration, the electrodes are located on the inner and outer walls of the sphere. Two principal modes of vibration were measured in this case—a volumetric expansion and contraction of the sphere at 633 kHz and a wall thickness mode at 13.4 MHz. For top-to-bottom poling, two external cap electrodes are located on the upper and lower surfaces of the sphere. In this case, the principal mode of vibration is an elliptical distortion of the sphere at 230 kHz. In both instances, the relative permittivity is quite high, approximately 1000.

When subject to a hydrostatic stress, this transducer exhibits a very large $d_h \cdot g_h$ product (figure of merit), on the order of 324,000 fm^2/N for radial poling and 100,000 fm^2/N for top-to-bottom poling. The amplification of d_h and figure of merit in BBs result purely from the spherical geometry. An applied hydrostatic pressure is transformed into radial and tangential stress components and amplified by a factor, which can be defined as the ratio of radius to wall thickness (r/t). The properties are reported to remain stable up to 7 MPa.

6.3. *Flexors/Benders*

The traditional flexor transducer consists of two piezoceramic plates (poled in opposing directions) which are cemented on each side of a central metal plate, or elastic shim. An enhanced voltage response comes from the sum of the contributions of the bending of the disk and the compression of the ceramic itself. Flexural piezoelectric elements are widely employed as ultrasonic sensors and accelerometers. Because of their dimensions, they are generally best suited for applications in the low ultrasonic frequency range. The conventional bender-type transducers are the bimorph and the unimorph [22]. The bimorph consists of two thin ceramic elements sandwiching a thin metal shim, whereas the unimorph is simply one thin ceramic element bonded to a thin metal plate. Both of these types are shown in Fig. 3.

A new type of flexural disk transducer is the monomorph, which consists of only a single flexible ceramic plate. An example of a monomorph is the RAINBOW. The rainbow transducer shows excellent promise as a low pressure (< 100 kPa) sensor and/or acoustic transmitter. RAINBOW is an acronym for Reduced And INternally Biased Oxide Wafer. As it is shown in Fig. 3, RAINBOW transducer consists of an electromechanically active layer, such as PZT, PMN, PLZT (lead lanthanum zirconate titanate), PBZT (lead barium zirconate titanate), or PSZT (lead stannate zirconate titanate), in direct contact with a lead-rich constraining layer [23]. This constraining layer is formed by exposing one side of a lead-containing ceramic to a reducing atmosphere at high temperature produced by placing a ceramic in contact with a carbon block. The reduction of the active layer occurs as a result of oxidation of the solid carbon block, first to $CO(g)$ then to $CO_2(g)$. This reduced layer is no longer piezoelectric, and is in fact, a good electrical conductor. Because of the thermal expansion mismatch between the reduced and oxide layer, a curvature develops in the structure, giving it a dome (or rainbow) shape, with the oxide layer in compression throughout its volume.

The RAINBOW disks are typically 0.5 mm thick and can range in diameter from one to tens of centimeters. When used as a pressure sensor, the dome needs to be fixed to a base plate; otherwise, the voltage response will only be equal to that of the bulk ceramic. Rainbows exhibit highly pressure-dependent properties but are extremely robust. As pressure increases, the dome gradually flattens, decreasing the bending contribution to g_h until it reaches the bulk value. For a 1 cm diameter sample bonded to a 1 mm thick base plate, a $d_h \cdot g_h$ product of 400 fm^2/N was measured at 2 MPa. A 3.16 cm diameter rainbow exhibited a $d_h \cdot g_h$ product of 10^7 fm^2/N ($g_h = 800$ mV·m/N) at pressures below about 100 kPa. At 1 MPa, it dropped to around 1000 fm^2/N, and beyond 2 MPa, it approached that of the bulk [24].

7. Piezoelectric Composite Sensors

Due to the low hydrostatic sensitivity of poled PZT, new approaches need to be taken to improve its performance. Examples of such approachs were the development of the RAINBOW and the BB transducers, as discussed in the previous section. An older

and more time-tested approach has been the incorporation of piezoceramics into composites. Composites provide the capability of utilizing the best aspects of each component in the composite while minimizing the poorest features. Most composite hydrophones consist of two phases—a stiff piezoceramic and a soft polymer. Newnham, et al., established the notation for describing the number of dimensions each phase is physically in contact with itself [25]. There are only ten ways in which two distinct components can be incorporated into a single composite. They are given the notation of 0-0, 1-0, 2-0, 3-0, 1-1, 2-1, 3-1, 2-2, 3-2, or 3-3 [26]. To date, eight different connectivity types of two-phase piezoelectric composites (piezocomposites) have been studied: 0-3, 1-3, 2-2, 2-3, 3-0, 3-1, 3-2, and 3-3. In the case of piezocomposites, the first number in the notation denotes the physical connectivity of the active phase and the second number refers to the physical connectivity of the passive phase. A schematic of these different connectivities is shown in Fig. 4.

Most ceramic-polymer composite sensors have been used as hydrophones. The purpose of the polymer is to absorb a portion the hydrostatic stress in either the transverse or longitudinal direction, effectively eliminating either the g_{33} or g_{31} contribution to the g_h of the poled ceramic. Extensive investigations have been performed to determine which ceramic-polymer connectivity configuration will provide the optimum hydrophone performance. In the following section, those piezoelectric ceramic-polymer composites and different approaches to fabricate them are discussed in details based on the connectivity of their constituent phases.

8. Piezoelectric Ceramic-Polymer Composites

8.1. Composites with 3-3 Connectivity

Composites with 3-3 connectivity were the first of the two phase composites to be investigated. They were initially fabricated by a technique known as the replamine process [27] which is the lost wax replication of a coral skeleton. Composites with this connectivity have reinforcement in the lateral directions which serves to further decouple negative contributions from lateral stresses [28]. Since then, additional technologies have been developed such as the fugitive phase, or BURPS (BURned out Polymer Spheres), process [29] which produces a porous three-dimensionally interconnected ceramic structure by sintering a compacted mixture of volatilizable plastic spheres and PZT powder. Mitsubishi Mining and Cement has developed several techniques for introducing connected porosity in PZT ceramics: reactive sintering, foaming agents, organic additives, and careful control of particle size and firing conditions. These pores can then be filled with silicone rubber [26,30]. A recent method used to produce 3-3 composites is the reticulated ceramic technology

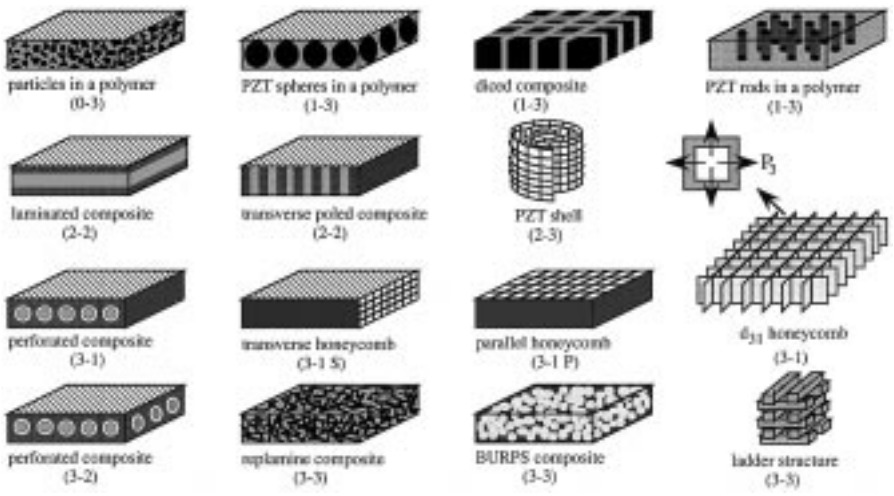

Fig. 4. Connectivity of constituent phases in piezoelectric ceramic-polymer composites.

[28]. Reticulated ceramics are created by coating an organic foam substrate (i.e. polyurethane) with a ceramic slurry, pyrolyzing the foam, and then sintering the ceramic. This group reports that by distorting, or elongating, the foam, it is possible to create a pseudo 1-3 interconnected configuration. They claim the advantages of enhanced hydrostatic response by the decoupling of the d_{31} and d_{32} responses as well as straightened ceramic pathways between electrodes, allowing for an increased level of poling and lateral reinforcement. In a more recent study from Rutgers University a new method to produce composites with 3-3 connectivity is reported [31]. In that study, ladder type and 3-D honeycomb type PZT-polymer composites are fabricated layer by layer using a fused deposition (FD) technique, which is a solid-freeform fabrication technique using computer aided design. This new FD technique leads to improved 3-3 composites of the same volume % PZT compared to replamine and BURPS techniques. A comparison of the properties from different fabrication techniques is presented in Table 5.

8.2. *Composites with 3-0 and 0-3 Connectivity*

The first 3-0 composites were fabricated by a tape casting technique. Fugitive ink was screen printed onto green PZT sheets which were subsequently stacked. When the ink and binder were burned out and the ceramic sintered, the resultant PZT block contained pores where the ink originally was. A second method for fabricating 3-0 composites consisted of hot pressing a mixture of large polymer spheres and PZT powder [26].

Composites with 0-3 connectivity consist of a random array of piezoelectric particles dispersed in a 3-D polymer matrix [32]. The primary advantage of these composites is their ability to be formed into shapes while remaining piezoelectrically active. These composites are manufactured commercially by NTK Technical Ceramic Division of the NGK Spark Plugs Corporation in Japan under the name *PiezoRubber* (NTK-306). PiezoRubber was developed by Banno and Saito and utilizes PT (lead titanate) rather than PZT in order to take advantage of the large piezoelectric anisotropy in PT [33].

The composite consists of fine $PbTiO_3$ particles of a very narrow size distribution (centered around 20 μm) embedded in a chloroprene polymer matrix [34]. A typical thickness of a 0-3 composite sheet is 500 μm. Good bonding between the particles and the rubber is necessary to achieve successful poling and subsequent good piezoelectric properties [35]. The use of a polymer with a high thermal coefficient of resistivity makes it possible to pole the composite at elevated temperatures by using the improved ceramic/polymer resistivity balance to give saturation poling while still retaining the high resistance and low loss at typical operating temperatures [32]. The g_h value reported by NTK for their *PiezoRubber* depends on the volume fraction of ceramic present and can be pressure insensitive up to 35 MPa [34–37]. One interesting application of 0-3 composites is a potential use as piezoelectric paint for use as a ''built-in'' vibration modal sensor [38]. Table 6 compares the properties of these types of composites.

8.3. *Composites with 3-1, 3-2, and 2-3 Connectivity*

Conventional composites exhibiting 3-1 and 3-2 connectivity consist of a PZT block with holes drilled through either one side (3-1) or both sides (3-2) in a direction perpendicular to the poled direction of the PZT. The holes are subsequently backfilled with

Table 5. Comparison of hydrostatic properties of composites with 3-3 connectivity

Technique	V_{PZT} (%)	d_h (pC/N)	g_h (mVm/N)	$d_h \cdot g_h$ (fm^2/N)	K^T	Matrix	Ref.
replamine	33	36	140	5040	50	silicone rubber	[26]
BURPS	50	260	100	26000	300	silicone rubber	[29]
BURPS	50	120	27	3200	500	epoxy[#]	[29]
Mitsubishi	50	90	50	4500	200	air or silicone rubber	[26,30]
reticulated	15	30	25	750	135	epoxy[#]	[28]

Dow Corning MDX-4-4210 Elastomer.
[#]Spurrs Epoxy.

Table 6. Comparison of hydrostatic properties of composites with 3-0 and 0-3 connectivity

Technique	d_h (pC/N)	g_h (mVm/N)	$d_h \cdot g_h$ (fm^2/N)	K^T	Matrix	Ref.
3-0 macrovoid	150	30	4500	560	PZT	[26]
0-3 PZT/polymer	28.3	32	900	100	silicone rubber	[40]
0-3 *PiezoRubber*	44	111	4884	38	elastomer	[36]

polymer. The 1-D or 2-D interconnected polymeric phases in the transverse direction reduce the g_{31} and g_{32} contributions to the hydrostatic voltage response by decreasing the stress coupling in the plane normal to the poled direction [39]. These two perforated PZT composite configurations are shown in Fig. 4. A negligible change in properties occurs up to 7 MPa. In 3-1 and 3-2 composites manufactured in this way, the dielectric constant, as well as the d_h and g_h coefficients are all functions of hole size, PZT thickness, poling technique, and center-to-center distance between adjacent holes [40].

Another type of 3-1 composite configuration utilizes a thin-walled 3-D interconnected piezoceramic frame (also known as a honeycomb). The first honeycombs were poled in directions either parallel or perpendicular (transverse) to the extrusion direction with the epoxy and PZT phases connected mechanically in parallel and series, respectively [26]. These honeycomb composite designs are shown in Fig. 4 as ''3-1 P'' and ''3-1 S'', respectively. Recently, a configuration has been devised where the ceramic frame is poled through the thickness of the frame walls using inner electrodes [41]. Thus, the composite operates in the d_{31} mode. This configuration of 3-1 composite is shown in Fig. 4 as the ''d_{31} honeycomb''. The high hydrostatic response comes from the sum of the individual responses of the three orthogonal directions of the frame. That makes this composite better than a capped cylinder, in which only the axial direction contributes to the hydrostatic response.

Two configurations of this composite have been fabricated. The first had the top and bottom of the frame covered with flat caps, leaving the empty space inside filled only with air. In this particular case, the d_{33} response of the piezoceramic is completely eliminated because the stress component perpendicular to the wall is zero.

The second configuration simply had the space within the frame infiltrated with a soft epoxy. Now, the d_{33} component is no longer suppressed because the stress component perpendicular to the wall is no longer zero. Nevertheless, since the frame is three dimensionally interconnected, the Poisson's ratio effect in the polymer phase (which is quite detrimental for 1-3 composites) is still greatly reduced.

The relic process, in combination with a weaving technique, has been developed to easily manufacture large area composites consisting of fine PZT fibers interconnected in two dimensions and embedded in a 3-D interconnected polymer matrix (2-3 connectivity). The relic process, reported by Rutgers University, starts with approximately 370 carbon fabric fibers 10 μm to 20 μm in diameter woven into yarns 37 picks per inch by 36 ends per inch [42]. The fabrics are soaked in a PZT slurry before being arranged into the desired structure. The carbon is then burned out and the resulting PZT relic is sintered to leave a structure similar to the original carbon template. A piezoelectric/polymer composite is subsequently formed by infiltrating this structure with epoxy. The weave and shell configurations both exhibit 2-3 connectivity. The weave has an interconnected checkerboard pattern. The shell consists of fibers rolled in a helical fashion around a center point. This composite configuration is shown in Fig. 4. A complete listing of properties for these composites is shown in Table 7.

8.4. Composites with 1-3 Connectivity

Unquestionably, the composites with 1-3 connectivity are the most extensively studied, understood, and utilized of all the two-phase connectivity types. This type of composite consists of individual PZT rods, or fibers, aligned in a direction parallel to the poling direction and surrounded by a polymer matrix. A decoupling of the d_{33} and d_{31} coefficients of the composite enhances the d_h. The rod diameter, rod spacing, composite thickness, volume percent of rods,

Table 7. Comparison of hydrostatic properties of composites with 3-1, 3-2, and 2-3 connectivity

Technique	d_h (pC/N)	g_h (mVm/N)	$d_h \cdot g_h$ (fm^2/N)	K^T	Matrix	Ref.
perforated 3-1	222	56	12300	450	epoxy	[40]
honeycomb (3-1 P)	20	5	100	450	polymer	[26]
honeycomb (3-1 S)	100	30	3000	400	polymer	[26]
d_{31} honeycomb	4700	1.02	4800	520	air (end-capped)	[41]
d_{31} honeycomb	4666	0.92	4316	570	polymer*	[41]
perforated 3-2	372	123	45700	340	air (sealed with polymer)	[40]
perforated 3-2	329	128	42000	290	epoxy	[40]
2-3 weave	80	65	5200	140	epoxy#	[42]
2-3 shell	80	60	4800	150	epoxy#	[42]

*polyurethane + 50% microballoons.
Spurrs epoxy.
#Eccogel epoxy.

and polymer compliance all influence the composite performance.

The first 1-3's were made from extruded PZT rods, ranging in diameter from 254 μm to 840 μm, which were aligned in a specially designed fixture which allowed for the epoxy to be poured around the rods [43]. Because of the labor intensive procedure, this technique does not lend itself well to mass production. The dice and fill technique [44] lends itself better to the mass production of smaller samples, but is too costly to meet the needs of large area coverage [35]. This technology involves the cutting of deep grooves into a solid block of PZT using a diamond saw. Square rods with width down to 50 μm are achievable with aspect ratios approaching twenty [45]. Different versions of 1-3 composites are shown in Fig. 4.

Cao, Zheng, and Cross [46] have shown that the stress transfer in 1-3 composites is accomplished through shear coupling at the interface between the ceramic and the polymer. The effectiveness of the stress transfer can be characterized by a stress amplification factor which depends upon the elastic properties of both phases, the ceramic content, and most importantly, the aspect ratio (radius/length) of the ceramic rods. These same parameters also affect the displacement uniformity over the surface of the composite [47]. When subject to a hydrostatic pressure, the stress applied in the transverse direction reduces the stress enhancement effect in the axial direction. This is due to the Poisson's ratio effect. When squeezed from both sides, the polymer bulges, pulling on the ceramic rods and trying to lengthen them. Essentially, this produces a contribution to the d_{31} of the composite from the d_{33} of the ceramic [48], which in turn lowers the d_h of the structure. Hence, under hydrostatic pressure, the stress amplification factor is practically reduced by a factor of $(1\text{-}2\sigma)$, where σ is Poisson's ratio. A more detailed discussion of this Poison's effect on the d_h of the composite is given by Smith [49].

A number of design modifications have been investigated to alleviate this problem. The incorporation of air pockets into the composite to absorb the lateral strain seems to be the preferred solution. This has been done by drilling air holes through the epoxy matrix in a direction parallel to the PZT rods [50], eliminating the interface between the PZT and the polymer matrix, allowing the stress transfer to instead be realized by armature plates located on the upper and lower surfaces of the composite [51], introducing pores or hollow glass spheres into the polymer matrix [52], and lastly, utilizing hollow, radially poled PZT tubes, which operate in the d_{31} mode instead of the d_{33} mode as in the case of rods [53,54]. Introducing a softer polymer matrix between the PZT rod and the harder epoxy has also been investigated [55] as well as incorporating glass fibers in the lateral direction to support the transverse direction stress [52]. Capping the rods serves to distribute the stress more uniformly over the active PZT surface and further decreases coupling of the Poisson stress components in the plane normal to the poled direction [56].

Square rods can give rise to undesirable inter-post resonant activity. This problem can be alleviated if circular or irregularly shaped rods are used instead [50]. By dicing a honeycomb configuration, ''**+**'',

''**L**'', and ''**T**'' shapes were easily fabricated [42]. Materials Systems Inc. has developed new technology for the mass production of large area 1-3 composites using an injection molding process [57]. This process is capable of producing arrays with rod diameters $< 100\,\mu$m. It is also possible to easily vary the PZT element type, layout, and shape. A comparison of the properties of various 1-3 composite designs is provided in Table 8.

8.5. *Composites with 2-2 Connectivity*

For large area acoustic projectors, it is necessary to generate large surface displacements while operating at a moderate driving voltage to get high radiative power over a wide frequency range. The 1-3 type composites often cannot meet these requirements. In addition, the d_h coefficient is limited by the longitudinal piezoelectric strain coefficient d_{33}. This can be alleviated by increasing the thickness, but at the cost of a higher electrical impedance. As in the case of the 1-3 composites, the strain profile across the surface of a 2-2 composite with a lamellar configuration is inhomogeneous due to the different elastic stiffnesses of the two components. The stress transfer between the two phases depends on the volume percent of active component as well as the aspect ratio of the two components [58]. Pressure induced depolarization can also become serious in a composite with low piezoelectric content. The 1-3 tubular composites operate in the d_{31} mode and do not depole under high pressures. Unfortunately, their manufacturing cost is high. The 2-2 piezocomposite operating in the transverse d_{31} mode possesses the advantages of the PZT tubular composite but with lower manufacturing costs and a simpler fabrication process [59]. This composite has thin piezoelectric plates forming a parallel array imbedded in a polymer matrix. The ceramic plates are electroded over the side faces with the polarization direction parallel to the acoustic radiation plane, i.e. they are transversely poled (TP). From Table 9, it can be seen that this new transverse operating mode 2-2 composite exhibits much better performance than the conventional longitudinal mode 2-2 designs, which are simply layers of PZT sandwiched between layers of polymer [42,59].

9. Piezoelectric Ceramic-metal Composites

Ceramic-metal composites are generally characterized by their simple designs and robustness. In these composites, metal faceplates, shells, or caps are coupled to both the active ceramic as well as the surrounding medium and are the means by which the incident stress is transferred to the ceramic. The best ceramic-metal composite sensors are the flextensional-type transducers. The term ''flextensional'' is in fact derived from a combination of the two words describing how the transducer works: the flexural vibration of the metal shell causes an extensional (or contractional) vibration of the piezoelectric element [60]. Flextensional transducers are typically quite large, in terms of both size and weight. The ''moonie'' and ''cymbal'' type transducers are miniaturized versions of flextensionals.

Table 8. Comparison of hydrostatic properties of composites with 1-3 connectivity

Technique	d_h (pC/N)	g_h (mVm/N)	$d_h \cdot g_h$ (fm^2/N)	K^T	Matrix	Ref.
PZT particles	29	32	900	100	polymer	[26]
PZT spheres	23	4	96	410	polymer	[26]
extruded rods	176	239	42064	83	polyurethane	[40]
dice & fill	52	18	935	330	polymer	[56]
w/ glass rods	203	220	44700	104	polyurethane*	[52]
w/ 2 polymers	288	78	22464	416	polymer#	[55]
''T'' diced honeycomb	75	15	1125	660	spurrs epoxy	[42]
PZT tubes	5502	1.2	6389	2922	spurrs epoxy	[53]
sonopanel	268	66	17688	460	polyurethane	[57]

*10% foamed.
air backing inside the tubes.
#polycarbonate matrix with epoxy interface between the PZT and the matrix.

Table 9. Comparison of hydrostatic properties of composites with 2-2 connectivity

Technique	d_h (pC/N)	g_h (mVm/N)	$d_h \cdot g_h$ (fm^2/N)	K^T	Matrix	Ref.
2-2 laminate	50	16.6	830	340	epoxy	[59]
2-2 (TP)	6000	5	30000	136	polyurethane	[59]
2-2 tape cast	25	10	250	300	spurrs epoxy	[42]

The moonie and cymbal transducers possess 2-(0)-2 connectivity. These transducers consist of a poled piezoelectric disk (fully electroded on each face) which is sandwiched between two metal endcaps, each containing a shallow air-filled cavity on their inner surface. In the case of the moonie, the cavities are in the shape of a half moon, whereas the cymbal has a truncated cone-shaped cavity (Fig. 5). The presence of these cavities allows the metal caps to serve as mechanical transformers for transforming and amplifying a portion of the incident axial-direction stress into tangential and radial stresses of opposite sign. Thus, the d_{31} and d_{33} contributions of the PZT now add together (rather than subtracting) in the effective d_h of the device [61]. For a moonie transducer 12.7 mm in diameter with a brass cap thickness of 0.3 mm, cavity diameter of 9 mm, and maximum cavity depth of 200 μm, an effective d_{33} coefficient of about 9000 pC/N has been reported [62]. In addition, a $d_h \cdot g_h$ product exceeding 50,000 fm^2/N is achievable [63]. A cymbal transducer, on the other hand, with brass caps 0.20 mm thick, cavity diameter of 9 mm, and maximum cavity depth of 200 μm will exhibit an effective d_{33} coefficient of at least 15000 pC/N [64] and a $d_h \cdot g_h$ product upwards of 100,000 fm^2/N [61]. The higher sensitivity in the case of the cymbal as compared to the moonie is at a cost of an increase in pressure dependence on its performance [61].

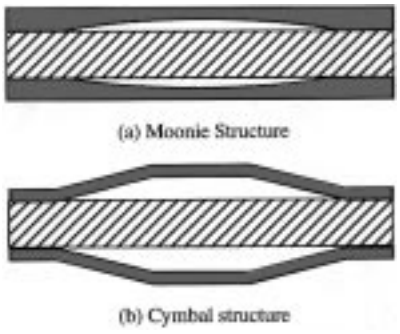

Fig. 5. Cross-sectional views of the (a) moonie and (b) cymbal transducers. The dark areas represent the caps, and the hatched areas the PZT disk.

10. Future Trends

Since the 1950s, lead oxide based compounds have been the leading materials for piezoelectric transducers due to their excellent dielectric and piezoelectric properties. However, with the increased public awareness on health concerns associated with lead and the recent changes in environmental policies, lead containing materials are now perceived as a health hazard. Therefore, increased research activity on Pb-free piezoelectric materials, in addition to the current intense efforts, are expected in the future. Additionally, research on piezoelectric single crystals in which very high strains can be induced, as in the recent example of PZN-PT and PMN-PT [65], and other lead-based as well as lead-free morphotropic phase boundary materials would be expected to continue yielding commercially available materials. An additional application which is gaining importance is the need for and the use of piezoelectric materials at cryogenic temperatures in outer space. Deep ocean exploration will also require highly sensitive piezoelectric materials which can operate at low temperatures ($\sim 4^\circ$C) and under high hydrostatic pressures (20 MPa). Most importantly, ferroelectric thin films are expected to form a major part of piezoelectric device applications.

11. Summary

Beginning with the discovery of ferroelectricity in $BaTiO_3$ and with the development of applications such as, electroacoustic transformers, signal processing devices, actuators and sensors piezoelectric materials have became an important part of engineering applications, as well as daily life. This is

evidenced by a review of piezoelectric sensors and sensors materials and an examination of the properties of the most common piezoelectric ceramic material: PZT, as well as other piezoelectric ceramics and single crystals. Several sensor configurations can be prepared from bulk ceramics as can piezoelectric ceramic—polymer composite sensors described by the connectivity of their constituent phases. A wide range of hydrophone figure of merit ($d_h \cdot g_h$) can be engineered through these sensor configurations. Recent examples of piezoelectric ceramic—metal composite sensors, and the future trends in the area of piezoelectric sensors show that piezoelectric sensors have established a solid presence in our daily life from ultrasound applications in medicine, to underwater ultrasound in military and civilian applications, to smart sensor systems in automobiles, to non-destructive testing in industry. They will continue to increase their impact even further with emerging technologies, improved material properties, and with an increased understanding of piezoelectric and ferroelectric phenomena.

Acknowledgment

A major part of the research on piezoelectric sensors and sensor materials at Materials Research Laboratory at The Pennsylvania State University has been supported by the Office of Naval Research (ONR) and National Science Foundation (NSF). The authors would like to thank for their financial support.

References

1. R. Maines, *Sensors*, **6**, 26 (1989).
2. D. Damjanovic and R.E. Newnham, *J. Intell. Mater. Struct.*, **3**, 190 (1992).
3. R. Barrett and F. Wilcoxon, *Sensors*, **10**, 16 (1993).
4. T. Furukawa, *Key Engineering Materials*, **92–93**, 15–30 (1994).
5. R.E. Newnham, *MRS Bulletin*, **22**, 20 (1997).
6. A.J. Moulson and J.M. Herbert, *Electroceramics* (Chapman & Hall, New York, 1992), p. 266.
7. H. Jaffe and D. Berlincourt, *Proc., IEEE*, **53**, 1372 (1965).
8. G.H. Haertling, in *Ceramic Materials for Electronics, Processing, Properties, and Applications*, edited by R.C. Buchanan (Marcel Dekkar, New York, 1986). p. 165.
9. B. Jaffe, W.R. Cook, and H. Jaffe, *Piezoelectric Ceramics* (Academic Press, New York, 1971), p. 148.
10. D. Berlincourt, *J. Acoust. Soc. Am.*, **70**, 1586 (1981).
11. A.S. Bhalla and R.Y. Ting, *Sensors and Materials*, **4**, 181 (1988).
12. T.B. Gabrielson, Presented at tha 1997 ONR Transducer Materials and Transducers Workshop, (The Pennsylvania State University, April 1997).
13. O.B. Wilson, *Introduction to the Theory and Design of Sonar Transducers* (Peninsula Publishing, Los Altos, CA, 1988), p. 65.
14. R.C. Turner, P.A. Fuirer, R.E. Newnham, and T.R. Shrout, *Appl. Acoustics*, **41**, 299–324 (1994).
15. T. Ikeda, *Fundamentals of Piezoelectricity* (Oxford University Press, New York, NY, 1990), p. 209.
16. K.M. Rittenmyer and R.Y. Ting, in *Electronic Materials: Technology, Here and Now*, edited by R. Keyson, D. Basiulis, and B. Woon (Society for the Advancement of Material & Process Engineering, 1991), p.24.
17. J.A. Gallego-Juarez, *J. Phys. E: Sci. Instrum.*, **22**, 804 (1989),
18. K.A. Klicker, J.V. Biggers, and R.E. Newnham, *J. Am. Ceram. Soc.*, **64**, 5–9 (1981).
19. O.B. Wilson, *Introduction to the Theory and Design of Sonar Transducers* (Peninsula Publishing, Los Altos, CA, 1988). p. 124.
20. J.T. Fielding, Jr., D. Smith, R.J. Meyer, Jr., S. Trolier-McKinstry, and R.E. Newnham, in *Proc. 9th IEEE Intl. Symp. Apps. Ferroelectrics*, edited by R.K. Pandey, M. Liu, and A. Safari (IEEE, New York, 1995), p. 202.
21. S. Alkoy, A. Dogan, A-C. Hladky, P. Langlet, J.K. Cochran, and R.E. Newnham, *IEEE Trans. UFFC*, **44**, 1067 (1997).
22. K. Uchino, *Piezoelectric Actuators and Ultrasonic Motors* (Klewer Academic Publishers, Boston, 1997).
23. G.H. Haertling, *Am. Ceram. Soc. Bull.*, **73**, 93 (1994).
24. S. Sherrit, H.D. Wiederick, B.K. Mukherjee, and G.H. Haertling, in *Proc. 9th IEEE Intl. Symp. Apps. Ferroelectrics*, edited by R.K. Pandey, M. Liu, and A. Safari (IEEE, New York, 1995), p. 390.
25. R.E. Newnham, D.P. Skinner, and L.E. Cross, *Mat. Res. Bull.*, **13**, 525 (1978).
26. T.R. Gururaja, A. Safari, R.E. Newnham, and L.E. Cross, in *Electronic Ceramics: Properties, Devices, and Applications*, edited by L.M. Levinson (Marcel Dekkar, New York, 1988), p. 92.
27. D.P. Skinner, R.E. Newnham, and L.E. Cross, *Mat. Res. Bull.*, **13**, 599 (1978).
28. M.J. Creedon, S. Gopalakrishnan, and W.A. Schulze, in *Proc. 9th IEEE Intl. Symp. Apps. Ferroelectrics*, edited by R.K. Pandey, M. Liu, and A. Safari (IEEE, New York, 1995), p. 299.
29. K. Rittenmyer, T. Shrout, W.A. Schulze, and R.E. Newnham, *Ferroelectrics*, **41**, 189–195 (1982).
30. K. Hikita, K. Yamada, M. Nishioka, and M. Ono, *Ferroelectrics*, **49**, 265–272 (1983).
31. A. Bandyopadhyay, R.K. Panda, V.F. Janas, M.K. Agarwala, S.C. Danforth, and A. Safari, *J. Am. Ceram. Soc.*, **80**, 1366–1372 (1997).
32. R.C. Twiney, *Adv. Mater.*, **4**, 819 (1992).
33. H. Banno, *Ferroelectrics*, **50**, 3 (1983).
34. R.Y. Ting, *IEEE Trans. Inst. Msmt.*, **41**, 64 (1992).
35. R.Y. Ting, *Appl. Acoustics*, **41**, 325 (1994).
36. R.Y. Ting, and F.G. Geil, in *1990 IEEE 7th Intl. Symp. App. Ferroelectrics* (IEEE, New York, 1991), p. 14.

37. R.Y. Ting, *Ferroelectrics*, **102**, 215 (1990).
38. S. Egusa and N. Iwasawa, *J. Intell. Mater. Sys. Struct.*, **5**, 140 (1994).
39. R.E. Newnham, J.F. Fernandez, K.A. Markowski, J.T. Fielding, A. Dogan, and J. Wallis, *Mat. Res. Soc. Proc.*, **360**, 33 (1995).
40. A. Safari, R.E. Newnham, L.E. Cross, and W.A. Schulze, *Ferroelectrics*, **41**, 197–205 (1982).
41. Q.M. Zhang, H. Wang, J. Zhao, J.T. Fielding, R.E. Newnham, and L.E. Cross, *IEEE Trans. UFFC*, **43**, 36 (1996).
42. V.F. Janas, S.M. Ting, S.S. Livneh, F.R. Walker, R. Schaeffer, T.F. McNulty, and A. Safari, in *Proc. 9th IEEE Intl. Symp. Apps. Ferroelectrics*, edited by R.K. Pandey, M. Liu, and A. Safari (IEEE, New York, 1995), p. 295.
43. K.A. Klicker, J.V. Biggers, and R.E. Newnham, *J. Am. Ceram. Soc.*, **64**, 5 (1981).
44. W.A. Smith, *SPIE*, **1733**, 3 (1992).
45. W.A. Smith and A.A. Shaulov, *Ferroelectrics*, **87**, 309 (1992).
46. W. Cao, Q.M. Zhang, and L.E. Cross, *J. Appl. Phys.*, **72**, 5814 (1992).
47. W. Cao, *Ceramic Engineering and Science Proc.*, **17**, 83 (1996).
48. W.A. Smith. in *1990 IEEE 7th Intl. Symp. Apps. Ferroelectrics*, (IEEE, New York, 1990), p. 145.
49. W.A. Smith, *IEEE Trans. UFFC*, **40**, 41–49 (1993).
50. J.A. Hossack, and R.L. Bedi, *Key Engr. Mater.*, **92–93**, 301 (1994).
51. L. Eyraud, C. Richard, and D. Guyomar, *in 1994 Ultrasonic Symposium Proceedings*, edited by M. Levy, S.C. Schneider, and B.R. McAvoy (IEEE, New York, 1994), p. 929.
52. M.J. Haun, R.E. Newnham, and W.A. Schulze, *Adv. Ceram. Mater.*, **1**, 361 (1986).
53. Q.M. Zhang, H. Wang, and L.E. Cross, *J. Mater. Sci.*, **28**, 3962 (1993).
54. J. Chen, Q.M. Zhang, L.E. Cross, and M. Trottier, in *Proc. 9th IEEE Intl. Symp. Apps. Ferroelectrics*, edited by R.K. Pandey, M. Liu, and A. Safari (IEEE, New York, 1995), p. 746.
55. C. Kim, K.M. Rittenmyer, and M. Kahn, *Ferroelectrics*, **156**, 19 (1994).
56. R.Y. Ting, *Ferroelectrics*, **67**, 143 (1986).
57. L. Bowen, R. Gentilman, D. Fiore, H. Pham, W. Serwatka, C. Near, and B. Pazol, *Ferroelectrics*, **187**, 109 (1996).
58. W. Cao, Q.M. Zhang, and L.E. Cross, *IEEE Trans. UFFC*, **40**, 103 (1993).
59. Q.M. Zhang, J. Chen, H. Wang, J. Zhao, L.E. Cross, and M.C. Trottier, *IEEE Trans. UFFC*, **42**, 774 (1995).
60. K.D. Rolt, *J. Acoust. Soc. Am.*, **87**, 1340 (1990).
61. J.F. Tressler, A. Dogan, J.F. Fernandez, J.T. Fielding, Jr., K. Uchino, and R.E. Newnham, in *1995 IEEE Ultrasonics Symposium Proceedings*, edited by M. Levy, S.C. Schneider, and B.R. McAvoy (IEEE, Piscataway, NJ, 1995), p. 897.
62. K. Onitsuka, A. Dogan, J.F. Tressler, Q.C. Xu, S. Yoshikawa, and R.E. Newnham, *J. Intell. Mat. Sys. Struct.*, **6**, 447 (1995).
63. Q.C. Xu, S. Yoshikawa, J.R. Belsick, and R.E. Newnham, *IEEE Trans. UFFC*, **38**, 634 (1991).
64. A. Dogan, K. Uchino, and R.E. Newnham, *IEEE Trans. UFFC*, **44**, 597 (1997).
65. S.-E. Park and T.R. Shrout, *J. Appl. Phys.*, **82**, (4), 1804 (1997).
66. Y. Xu, *Ferroelectric Materials and Their Applications* (North-Holland, Amsterdam, The Netherlands, 1991), p. 217, 277
67. M.M. Choy, W.R. Cook, R.F.S. Hearmon, H. Jaffe, J. Jerphagnon, S.K. Kurtz, and S.T. Liu *Landolt-Börnstein Numerical Data and Functional Relationships in Science and Technology*, edited by K.-H. Hellwege and A.M. Hellwege, (Springer-Verlag, Heidelberg, New York, 1979), Vol. 11, p. 328
68. Morgan Matroc company product literature.